Supplemental Material for Dual-Band Polarization Control with Pairwise Positioning of Polarization Singularities in Metasurfaces

Chloe F. Doiron, Igal Brener, and Alexander Cerjan

I. EXPERIMENTAL MEASUREMENT SETUP

We performed all experimental measurements using a home-built reflectance setup depicted in Fig. S1.

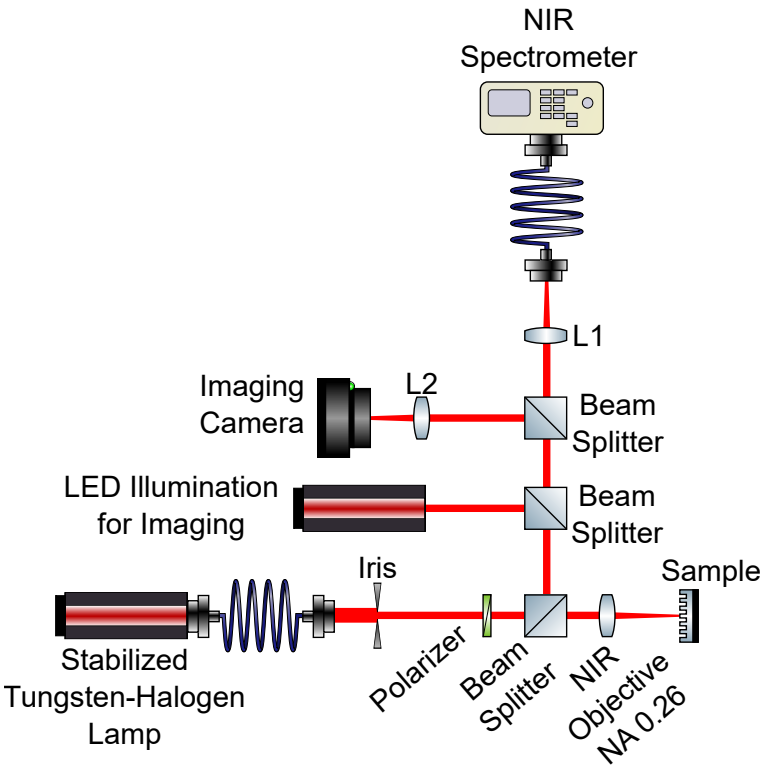

FIG. S1. Diagram of home-built setup used for reflectance measurements. The NIR objective has an entrance diameter of 12.5 mm and was operated in the under-filled condition with a 3.5 mm beam diameter.

II. SYMMETRY BREAKING OPERATIONS

An expanded schematic of symmetry breaking operations is presented in Fig. S2.

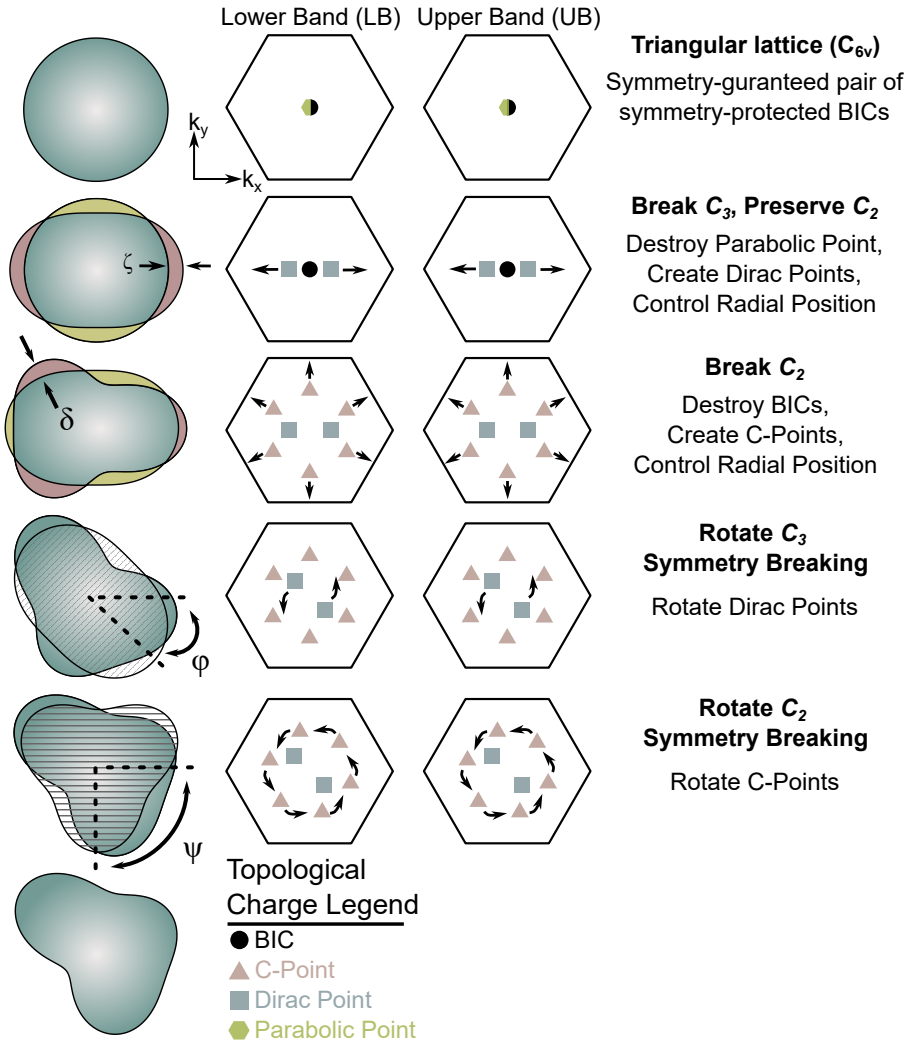

FIG. S2. Expanded schematic visualizing the relationship between symmetry breaking deformations and the positions of polarization singularities. When all symmetries of the triangular lattice are preserved, symmetry-guranteed pairs of BICs can occur. By breaking C_3 symmetry, the degeneracy is lifted resulting in the creation of two Dirac points. Similarly, breaking C_2 converts the BICs to quasi-BICs with finite lifetimes and therefore the creation of six C-points. Rotating the C_3 and C_2 symmetry breaking operation controls the rotational positions of the Dirac points and C-points respectively.

III. SEPARATED EIGENPOLARIZATION PLOTS

A modified version of Fig. 1 with the eigenpolarization ellipses from the two bands are plotted separately is provided in Fig. S3.

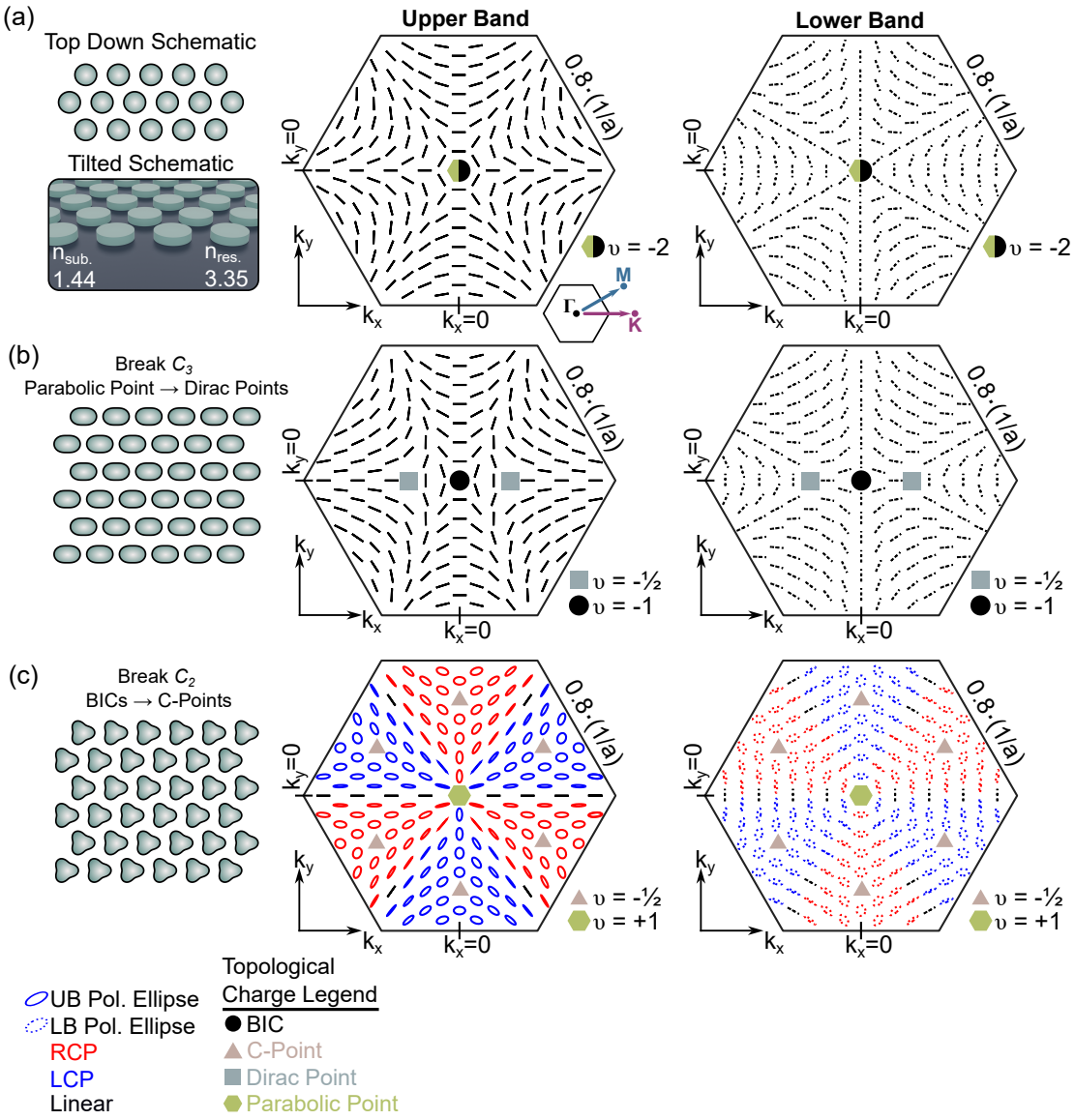

FIG. S3. Eigenpolarizations from Fig. 1 with the upper and lower bands plotted separately for (a) when all symmetries are preserved, (b) when a C_3 symmetry breaking deformation is applied, and (c) when a C_2 symmetry breaking deformation is applied. For the bands investigated by this work, when C_3 is preserved the polarization ellipses do not flip character when following the bands through the parabolic point (touching behavior). In comparison, when C_3 is broken, the polarization characters for the upper and lower bands flip (crossing behavior) when passing through the Dirac point. These results are consistent with other works studying parabolic degeneracies [1]. For bands closer to the diffraction limit, other conservation dynamics may occur changing the conditions of when touching or crossing behaviors occur.

IV. EIGENPOLARIZATION ANALYSIS

When using the guided mode expansion (GME) method to calculate the eigenmodes, we also calculate the complex radiative coupling rates to the far-field for each eigenmode for S- and P- polarizations (u_s and u_p respectively) for all allowed diffraction orders. Since we are operating below the diffraction limit, only the zeroth diffraction order is present. With these two complex coupling rates, we can define the polarization states of eigenmodes (eigenpolarizations) by projecting the complex radiative coupling rates onto the xy-plane [2] and calculating the stokes parameters with Eqns. 1-4. Together, these parameters completely define the eigenpolarization ellipse.

$$S_0 = |u_x|^2 + |u_y|^2 \tag{1}$$

$$S_1 = |u_x|^2 - |u_y|^2 \tag{2}$$

$$S_2 = 2\text{Re}(u_x u_y^*) \tag{3}$$

$$S_3 = -2\text{Im}(u_x u_y^*) \tag{4}$$

To experimentally characterize the eigenpolarizations, we can measure the relative coupling efficiency between a plane wave with a fixed input polarization and the eigenpolarization of the mode in the far-field. In general, the absolute coupling efficiency for coupling from far-field illumination to a system with one mode is given by Eq. 5 [3].

$$\eta = \frac{P_{\text{out}}}{P_{\text{in}}} = \text{Re}\left(\frac{(\int \mathbf{E}_{\text{mode}} \times \mathbf{H}_{\text{in}}^* \cdot d\mathbf{S})(\int \mathbf{E}_{\text{in}} \times \mathbf{H}_{\text{mode}}^* \cdot d\mathbf{S})}{\int \mathbf{E}_{\text{mode}} \times \mathbf{H}_{\text{mode}}^* \cdot d\mathbf{S}}\right) \frac{1}{\text{Re}(\int \mathbf{E}_{\text{in}} \times \mathbf{H}_{\text{in}}^* \cdot d\mathbf{S})} \tag{5}$$

Reflectance measurements with near normal incidence illumination (maximum angle of incidence was $4.3°$) and linear polarization, probe eigenpolarizations near the $\mathbf{\Gamma}$-point where they are nearly linear. In the case of coupling linear polarized illumination with a linear eigenpolarization Eq. 5 can be simplified to Eq. 6 where θ is the angle between the input polarization and nearly linear polarization ellipse major axis.

$$P_{\text{out}} = P_{\text{in}} \cdot \cos^2(\theta) \tag{6}$$

But, this relationship only holds when there are no other modes to couple into. When multiple modes are present, the coupling efficiency into the k-th mode is given in Eq. 7.

$$\eta_k = \frac{P_k}{P_{\text{in}}} = \text{Re}\left(\frac{(\int \mathbf{E}_k \times \mathbf{H}_{\text{in}}^* \cdot d\mathbf{S})(\int \mathbf{E}_{\text{in}} \times \mathbf{H}_k^* \cdot d\mathbf{S})}{\int \mathbf{E}_k \times \mathbf{H}_k^* \cdot d\mathbf{S}}\right) \frac{1}{\text{Re}(\int \mathbf{E}_{\text{in}} \times \mathbf{H}_{\text{in}}^* \cdot d\mathbf{S})} \tag{7}$$

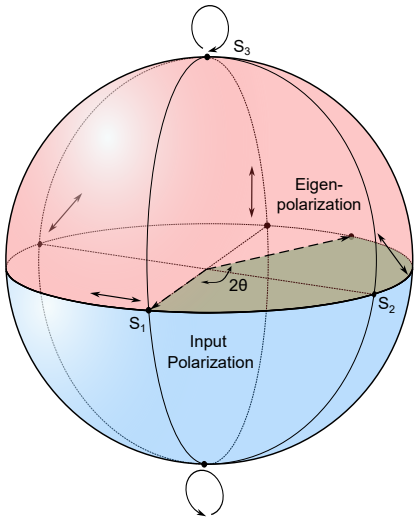

FIG. S4. Depiction of the input polarization state and eigenpolarization of the metasurface on the Poincaré sphere

Because the reflectance measurements only directly probe P_{out} it measures the reflectance effects of all modes, most notably low-Q modes at frequencies above and below the pair of quasi-BICs creating a background that needs to be accounted for leading to Eq. 8.

$$|P_{\text{out}} - P_{\text{background}}| \propto \cos^2(\theta) \tag{8}$$

An experimental demonstration of Eq. 8 is presented in Fig. S5.

While the measured reflectance behavior agrees well with simulations, the amplitude of the reflectance signal for the upper and lower band can differ significantly as seen in Fig. 4(d). This is most likely the effects of low Q-modes at frequencies above and below the pair of quasi-BICs. Future design methods could minimize the effects of the background modes to obtain a more consistence reflectance response.

V. ANALYSIS OF REFLECTANCE SPECTRA FOR DEFORMATION ROTATION

To quantify the behavior of polarization control, Q-factors, mode positions, and mode splittings we fit the experimentally measured reflectance spectra with two Fano line shapes and a polynomial background given in Equation 9.

$$a_1 \cdot \frac{(q_1 + (\omega - \omega_1))}{\left(\frac{\Gamma_1}{2}\right)^2 \left(1 + \frac{(\omega-\omega_1)}{(\frac{\Gamma_1}{2})^2}\right)} + a_2 \cdot \frac{(q_2 + (\omega - \omega_2))}{\left(\frac{\Gamma_2}{2}\right)^2 \left(1 + \frac{(\omega-\omega_2)}{(\frac{\Gamma_2}{2})^2}\right)} + c_0 + c_1 \cdot \omega + c_2 \cdot \omega^2 + c_3 \cdot \omega^3 \tag{9}$$

From these fits we are able to recover the mode positions (ω_1 and ω_2), mode splittings ($|\omega_1 - \omega_2|$), and Q-factors ($\frac{\omega_{1,2}}{\Gamma_{1,2}}$). From the recovered mode positions and mode splittings we calculated root-mean-square deviations ($\sqrt{\frac{1}{n}\sum_{i=1}^{n}(X_i - \bar{x})^2}$).

In the measured reflectance spectra, a deviation from Fano line shapes can be seen in Figures 3 and 4 when the input polarization is orthogonal to one of the modes occurring at $0°$, $90°$, and $180°$ for C_3 symmetry breaking deformations and $0°$, $30°$, and $60°$ for C_3 symmetry breaking deformations with the missing reflectance dips at the high energy side of the peaks. This can be attributed to performing reflectance measurements with a non-zero angular bandwidth ($\pm 4.3°$). In certain configurations, Fano line shapes can be obscured [4]. Because of this issue, we treat the integrated reflectance amplitudes at these points as baselines for Figures 3(d) and 4(d).

VI. POLARIZATION RESPONSE

To experimentally demonstrate the effect of input polarization on probing the eigenpolarization through reflectance measurements we selected the metasurface with symmetry breaking strengths of $\delta = 25\,\mathrm{nm}$, $\zeta = 30\,\mathrm{nm}$, and symmetry deformation angles $0°$ for both C_2 and C_3. We measured reflectance spectra with input polarization from $0°$ (horizontal in Fig. 3(a)) to $90°$ (vertical in Fig. 3(a)) [Fig. S5(a)]. We fit these spectra with a two Fano line shapes to recover the Q-factors and amplitudes as a function of polarization. As expected as the polarization is changed, we observed no effect on the Q-factors [Fig. S5(b)] since only mode coupling efficiency is being varied and not the lifetime. Similarly, because we are adjusting the coupling efficiency we observed the expected $\cos^2(\theta)$ dependence [Fig. S5(c)]. Similarly, we measured reflectance spectra of the metasurface when illuminated with right hand circularly polarized (RCP) light [Fig. S6]. As expected, both the upper and lower bands are simultaneously observable with similar Q-factors (141 for the upper band and 163 for the lower band).

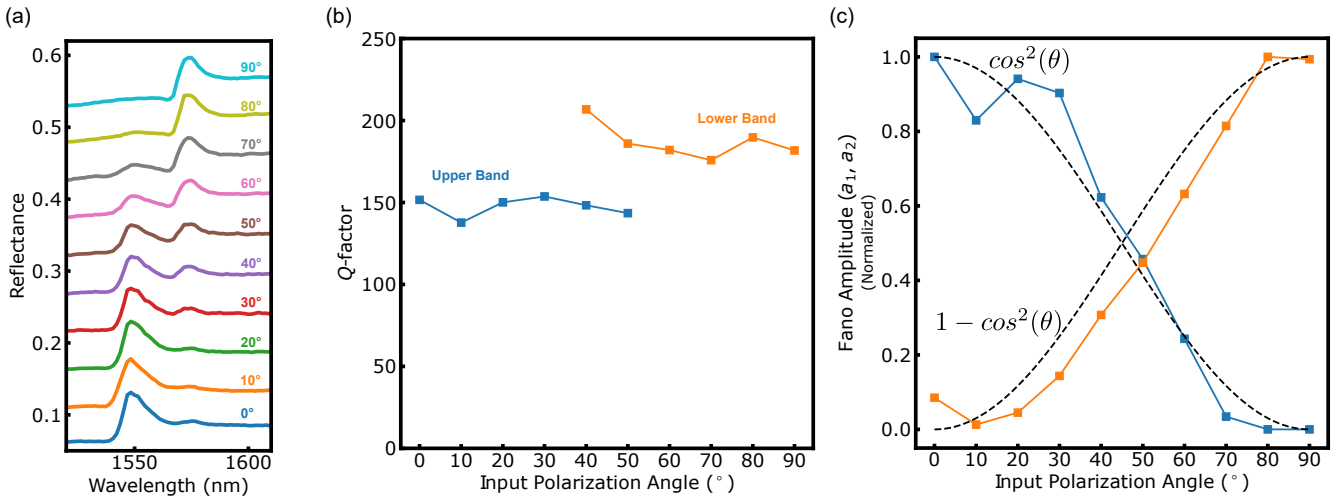

FIG. S5. (a) Reflectance spectra for input polarizations from 0° (horizontal in Fig. 3(a)) to 90°. The metasurface with symmetry breaking strengths were $\delta = 25\,\mathrm{nm}$, $\zeta = 30\,\mathrm{nm}$, and symmetry deformation angles 0° for both C_2 and C_3. (b) Q-factors for the upper and lower band extracted from the reflectance spectra. (c) Fano line shape amplitudes extracted from the reflectance measurements.

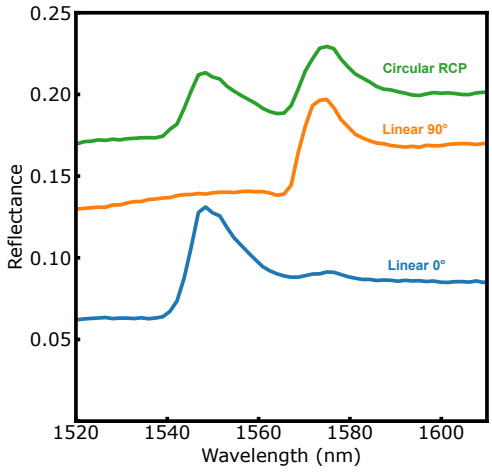

FIG. S6. Reflectance spectra for input linear polarization 0° (horizontal in Fig. 3(a)), linear polarization 90°, and right handed circular polarizations.

VII. SIMULTANEOUS ROTATIONS OF C_3 AND C_2 SYMMETRY BREAKING DEFORMATIONS

Simulated integrated reflectance values for simultaneous rotations of C_3 and C_2 symmetry breaking deformations are presented in Fig. S7. With the rotation of both symmetry breaking

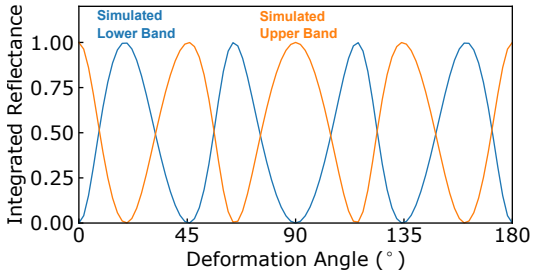

FIG. S7. Simulated integrated reflectance values for simultaneous rotations of C_3 and C_2 symmetry breaking deformations.

deformations, both Dirac points and C-points will rotate, causing the eigenpolarizations for the upper and lower bands to rotate four times as the deformations are rotated through $180°$.

[1] A. Chen, W. Liu, Y. Zhang, B. Wang, X. Liu, L. Shi, L. Lu, and J. Zi, Observing vortex polarization singularities at optical band degeneracies, Physical Review B **99**, 180101 (2019).

[2] Y. Zeng, G. Hu, K. Liu, Z. Tang, and C.-W. Qiu, Dynamics of topological polarization singularity in momentum space, Physical Review Letters **127**, 176101 (2021).

[3] G. Son, S. Han, J. Park, K. Kwon, and K. Yu, High-efficiency broadband light coupling between optical fibers and photonic integrated circuits, Nanophotonics **7**, 1845 (2018).

[4] Z. Geng, J. Theenhaus, B. K. Patra, J.-Y. Zheng, J. Busink, E. C. Garnett, and S. R. Rodriguez, Fano lineshapes and rabi splittings: Can they be artificially generated or obscured by the numerical aperture?, ACS photonics **8**, 1271 (2021).